IBRO Neuroscience Reports 10 (2021) 225–235

Contents lists available at ScienceDirect

IBRO Neuroscience Reports

journal homepage: www.sciencedirect.com/journal/IBRO-Neuroscience-Reports

Comparison of effect of crush or transection peripheral nerve lesion on lumbar spinal cord synaptic plasticity and microglial dynamics

Raquel M.P. Campos [a], Maria Carolina Barbosa-Silva [a], Victor T. Ribeiro-Resende [a,b,*]

[a] Instituto de Biofísica Carlos Chagas Filho, Laboratório de Neuroquímica, Universidade Federal do Rio de Janeiro, Rio de Janeiro, RJ 21941-902, Brazil
[b] Núcleo Multidisciplinar de Pesquisa em Biologia (Numpex-Bio), Campus de Duque de Caxias Geraldo Guerra Cidade, Universidade Federal do Rio de Janeiro, Duque de Caxias, RJ 25255-030, Brazil

ARTICLE INFO

Keywords:
Sciatic nerve
Lumbar spinal cord
Synaptic plasticity
Microglia

ABSTRACT

In an injury to the peripheral nervous system, the spinal cord and brain structure reorganize connections to optimize the function of the remaining parts. Many cell events are triggered in the spinal cord to support changes in the synaptic connections around motoneurons, where old connections are removed, and new ones created. Microglial cells are primitive macrophages that invade the central nervous system in early stages of neurodevelopment and have several functions, such as eliminating synapses. We investigated the synaptic plasticity after different types of peripheral (sciatic) nerve injury (crush or total transection), as well as the behavior of microglial cells for 2 weeks after a peripheral lesion. As expected, sciatic-nerve injury reduced motor performance in mice, but crushed animals regained partial motor control. Because of sciatic-nerve injury, pre-synaptic inputs decreased around the motoneurons in the ventro-lateral horn, while microglial cells increased around these cells. Microglial cells also exhibited altered morphology in both types of peripheral lesion, indicating a similar underlying mechanism of plasticity. To investigate the involvement of microglia in this scenario, microglial activation was modulated by daily administration of minocycline. The minocycline treatment directly affected the microglial response and impacted the synapse rearrangement in the spinal cord. Together, these results demonstrate that microglia cells are involved in synaptic plasticity in the lumbar spinal cord in both nerve-injury scenarios.

Summary of statement: Here, we demonstrated that acute plasticity in the lumbar spinal cord (LSC) did not differ between crush and transection of peripheral nerve, and that microglial reactivity in the LSC was important after both injury types.

1. Introduction

Peripheral Nervous System (PNS) injury leads to a homeostatic change in the Central Nervous System (CNS), as observed through different approaches (Emirandetti et al., 2006, 2010; Spejo et al., 2013; Tyzack et al., 2014; Arbat-Plana et al., 2015). Among the sequence of cell processes triggered after axonal disruption, synaptic rearrangement at the spinal cord level and reduction of synaptic inputs to motoneurons are prominent (Blinzinger and Kreutzberg, 1968). This rearrangement can be explained as an attempt to promote neural viability, axon regeneration, and target reinnervation (Wolpaw and Carp, 2006; Emirandetti et al., 2010; Spejo et al., 2013; Arbat-Plana et al., 2015).

In a case of axon regeneration and target reinnervation, as occurs after axonotmesis, there is a second wave of synaptic rearrangement, with partial recovery of previous connections, a consequence of reintegration of the member in the somatotopic representation (Seddon, 1943; Sunderland, 1951; Wall et al., 1984, 1986; Alvarez et al., 2011; Schultz et al., 2017). Knowledge of how and when the second wave of plasticity occurs is important, especially for therapeutic purposes, since restoration of motor and sensory functions of limbs after peripheral nerve lesion depends not only on reinnervating the target but also on the CNS adapting to motor and sensory feedback (Wall et al., 1984, 1986).

Part of the CNS plasticity mechanisms involves pruning of synapses. This pruning is organized by glial cells in several contexts, including in the CNS after PNS insult (Emirandetti et al., 2006, 2010). Recent studies have found that the mechanisms underlying this plasticity also include microglial cells, with their phagocytic capacity. Microglia are myeloid cells that originate in the yolk sac and infiltrate the CNS during

* Correspondence to: Instituto de Biofísica Carlos Chagas Filho, Universidade Federal do Rio de Janeiro, Rio de Janeiro, RJ 21941-902, Brazil.
E-mail address: vtulio@biof.ufrj.br (V.T. Ribeiro-Resende).

https://doi.org/10.1016/j.ibneur.2021.05.002
Received 9 March 2021; Received in revised form 10 May 2021; Accepted 12 May 2021
Available online 16 May 2021

embryogenesis (Ginhoux et al., 2010). For several decades, the only function attributed to microglial cells was immunological, to protect the CNS by eliminating pathogens (Prinz et al., 2011). New functions have recently been attributed to these cells, since they are sensors of the environment and important players in CNS homeostasis (Gomez-Nicola and Perry, 2015; Jones and Lynch, 2015; Xavier et al., 2014; Orihuela et al., 2016). These cells have an important role in the refinement of synaptic circuits during the development and post-natal periods, as observed in the dorsal lateral geniculate nucleus (dLGN) (Stevens et al., 2007). Synapse elimination, or pruning, in different CNS regions can also occur in adulthood and include participation by microglial cells (Wake et al., 2009; Emirandetti et al., 2010; Hundeshagen et al., 2013; Arbat-Plana et al., 2015; Li et al., 2016).

As is well understood, microglia cells have a spectrum of activation; each phenotype has different characteristics, such as morphology and the molecules that it expresses (Biber et al., 2007; Mecha et al., 2016; Bastien and Lacroix, 2014; Stratoulias et al., 2019). This spectrum includes microglia involved in pro-inflammation that secrete several molecules, such as tumor necrosis factor alpha (TNF-α), interleukin 6 (IL-6), and inducible nitric-oxide synthase (iNOS) (Trapp et al., 2007; Jones and Lynch, 2015; Li et al., 2016; Lisi et al., 2017; Xu et al., 2017). Another phenotype, involved in repair and neuroprotection, releases anti-inflammatory mediators such as IL-4, IL-13, arginase, and TNF, and neurotrophic factors such as BDNF (Jones and Lynch, 2015; Xavier et al., 2014; Xu et al., 2017). The morphology of microglial cells can vary across the CNS structure, but the repair phenotype has been described as more ramified compared to when these cells are compromised in a pro-inflammatory state (Walker et al., 2014; Jones and Lynch, 2015; Mecha et al., 2016; Li et al., 2016; Spittau, 2017).

Emirandetti and collaborators (2010) observed an increased number of microglial cells positive for iNOS in the spinal cord after sciatic transection at the same time-point, where synaptophysin was decreased in the same field. In mice lacking iNOS, the authors found that a reduced rate of synapse pruning was correlated with high percentages of resting microglial cells. Therefore, microglial cells and pro-inflammatory cytokines have been associated with the synaptic plasticity following peripheral nerve injury (Hundeshagen et al., 2013; Spejo et al., 2013; Arbat-Plana et al., 2015; Li et al., 2016).

Here, we investigated whether different types of peripheral nerve injury, i.e., crush or total transection, could affect the synaptic plasticity in the lumbar spinal cord (LSC) and the microglial response in acute periods following sciatic nerve injury. We also investigated whether changes in the microglial phenotype would regulate synaptic plasticity in the spinal cord, and the consequences for hindlimb motor function.

2. Experimental procedures

2.1. Animals

All experiments were performed following the National Institutes of Health Guidelines for the Care and Use of Laboratory Animals and were approved by the Ethics Committee for the Use of Animals in Research from the Universidade Federal do Rio de Janeiro (CEUA IBCCF protocol #175-018). For this study, two- to three-month-old male C57Bl6 mice ($n = 155$) were used, as in previous studies (Emirandetti et al., 2006, 2010; Hundeshagen et al., 2013; Yamada and Jinno, 2013; Tyzack et al., 2014; Li et al., 2016). The animals were bred at our institution's rodent facility and housed with free access to food and water. The mice were divided into 3 main groups: Control (unlesioned) ($n = 13$), Crush ($n = 40$), and Transection (n = 36).

2.2. Sciatic-nerve injury

Mice from the Crush and Transection groups were anesthetized by intraperitoneal administration of ketamine (20 mg/kg) and xylazine (15 mg/kg). The hind paw was shaved, an incision parallel to the femur was made with a scalpel, and the right sciatic nerve was exposed with the help of surgical tweezers. For the Crush group, the sciatic was crushed for 15 s with a pair of jeweler's forceps (#4). Transected mice had a 0.3-mm section from the nerve removed with micro-scissors. The muscles and skin incision were sutured using 0.3 surgical nylon thread. The mice received no analgesic after surgery.

2.3. Pharmacology

Minocycline powder (Sigma Catalog #M9511) was diluted in sterile phosphate buffer every 2 days. Mice received minocycline intraperitoneally, 45 mg/kg once a day, with 24 h between doses (Nikodemova et al., 2007; Scholz et al., 2015; Wang et al., 2015; Ahmed et al., 2017), starting 6 h before the sciatic-nerve injury until the day of their euthanasia (Fig. 1). The animals treated with minocycline were separated into groups: Control+Minocycline ($n = 10$), Crush+Minocycline ($n = 28$) and Transection+Minocycline ($n = 28$).

2.4. Sciatic functional index

Motor performance was evaluated using the CatWalk apparatus (Noldus). All mice walked over a platform with pressure sensors twice a day, and were evaluated 1, 4, 7, and 14 days after lesion. The internal toe spread, and the lengths of both hind paws were measured, and the Sciatic Functional Index (SFI) was calculated as described by Inserra and colleagues (1998).

2.5. Histology and immunofluorescence

Mice were euthanized with I.P. administration of ketamine (40 mg/kg) and xylazine (30 mg/kg), twice the dose used for surgery anesthesia, 1, 4, 7, or 14 days after lesion (DAL). The spinal cord from L3 to S2 was dissected and fixed by immersion in a 4% paraformaldehyde solution (Millipore #158127; in 0.1 M phosphate buffer, pH 7.4) for 7 days. The tissue was cryoprotected with a sucrose gradient (10–30% in 0.2 M phosphate buffer; Sigma #S0389) and mounted using Tissue-Tek O.C.T. Compound (Sakura Finetechnical, Tokyo, Japan). Frozen transverse sections of spinal cord were sliced at 12 μm, using a cryostat (Leica CM, 3050 s Leica Microsystems Nussloch GmbH), mounted on slides precoated with 1% gelatin, and stored at −20 °C.

For immunostaining, samples were washed 3 times for 5 min each with PBS containing 0.3% Triton X-100 and incubated with 5% or 20% NGS for 1 h at room temperature (RT), followed by incubation with primary antibodies overnight at 4 °C and 3 washes with PBS (5 min each). Finally, secondary antibodies were incubated in PBS containing 10% NGF for 2 h at RT, followed by 3 washes and DAPI (nuclear stain) (1:1000; Sigma #32670). Samples were covered with coverslips containing Vectashield (Vector). Primary antibodies used were mouse monoclonal anti-synaptophysin (1:100, Vector Laboratories #VP-S285) and rabbit polyclonal anti-Iba1 (1:200, Wako #019–19741). Secondary antibodies used were goat anti-mouse Alexa 594 (1:400, Thermo Fisher Scientific #A-31570) and goat anti-rabbit Alexa Fluor 594 (1:400, Life Technologies, Thermo Fisher Scientific #R37117).

2.6. Image analysis

Images from stained spinal cords ipsilateral to the nerve injury were obtained using an apotome microscope (Axio Imager M1, Zeiss, Oberkochen, Germany). For synaptophysin staining, 6 images from different sections of the ventral horn of each animal were taken with the same settings, using a 40 × objective and the same exposure time for DAPI (16 ms) and Synaptophysin (260 ms). Each photomicrograph included 3 or 4 motoneurons, which were identified by the large cell body and faint DAPI staining compared to the other cells in the image. A pool of 18–24 motoneurons were analyzed per animal. The photomicrographs were analyzed as described by Emirandetti et al. (2010). ImageJ

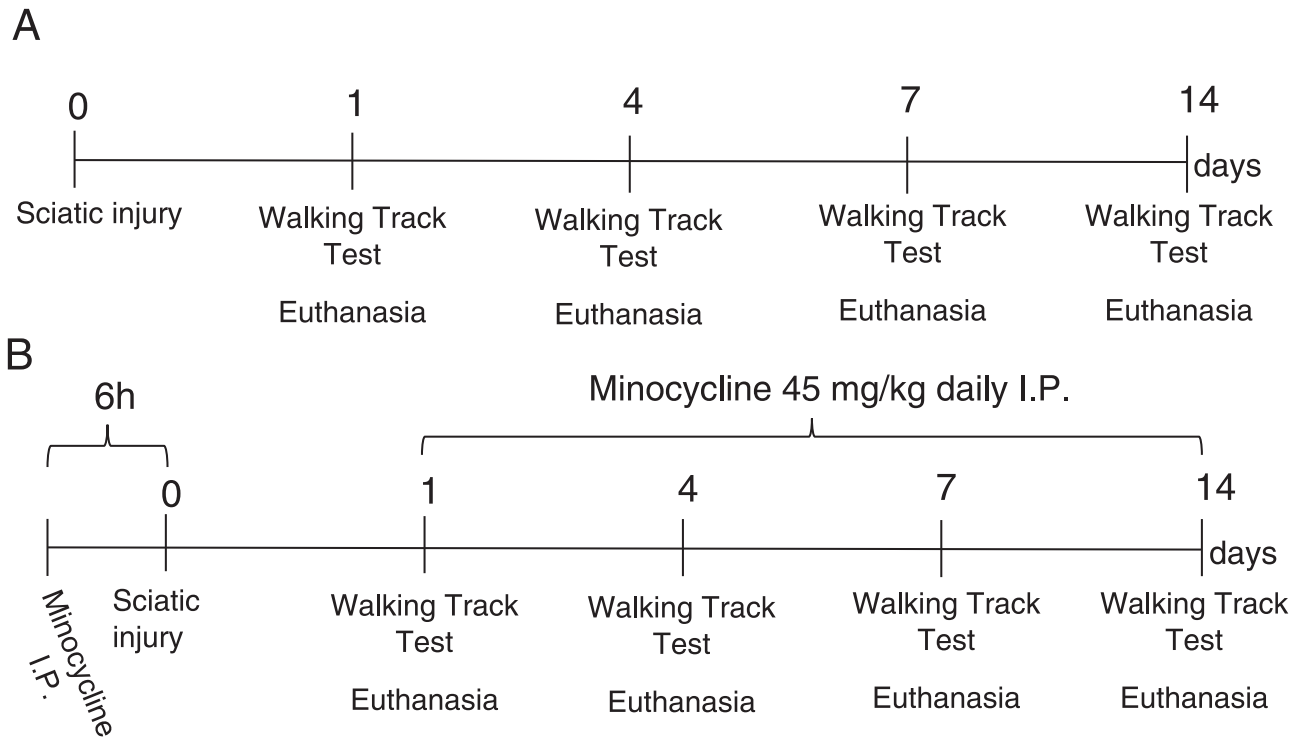

Fig. 1. Experimental design. (A) Timeline showing days following nerve injury in mice, where the walking-track test and the time of euthanasia are indicated. (B) Timeline showing the experimental design of the minocycline treatment, where the first dose was administered 6 h prior to the surgical procedure, followed by a dose every 24 h after the injury.

software (version 1.29, National Institutes of Health, USA) was used to measure the integrated density in pixels of 8 regions, with the perimeter close to 5 μm around each motoneuron cell body (Arbat-Plana et al., 2015). A mean of synaptic density in each neuron was calculated, and then the mean of the spinal cord from each animal.For quantitative analysis of microglial cell density, images of the complete LSC were taken using the mosaic mode and a 40 × objective. Four sections from each animal, stained with 2 different immunohistochemistry procedures, were used for the quantification and morphological analysis. The total number of Iba1 + cells on the ipsilateral side was calculated per area, using Zen software (Zeiss, Germany). The morphology of Iba-1 + cells of the ventral horn of the spinal cord ipsilateral to the sciatic lesion was analyzed using apotome-coupled fluorescence microscopy, at 400× magnification. Using the Maximum Intensity Projection tool, 3D images were converted to 2D. The photomicrograph was exported in TIFF format and morphological parameters were analyzed in ImageJ as described by Young and Morrison (2018), using a skeleton plugin, and in FIJI for Sholl analysis, as used by Rotterman et al. (2019) (Supplementary Figure 2). The morphology of a mean of 10 microglia per animal was analyzed. All analyses were done blinded, where one person acquired and coded the photomicrographs, and another person conducted the counting and analyses.

2.7. Western blot analysis

The L4–L6 regions of the spinal cord were removed and frozen in liquid nitrogen. The tissue was sonicated in lysis buffer (50 nM Tris base, 2 nM EDTA, and 2% SDS) and a protease inhibitor cocktail (Sigma #P2714), and the total protein concentration was quantified (Lowry et al., 1951). Western blotting was performed after 30 μg of protein extract from each tissue sample was electrophoresed in 12% polyacrylamide gel and electrotransferred to nitrocellulose membranes (Bio-Rad #1620115). The membranes were blocked for 1 h with 5% nonfat milk in Tris buffered saline (TBS) at room temperature, with shaking. Mouse monoclonal anti-synaptophysin (1:1000, Vector Laboratories #VP-S285) and mouse anti-alpha tubulin (1:10,000 Abcam #ab184613) were diluted in TBS and incubated overnight at 4 °C. Membranes were washed with TBS plus 0.02% Tween and goat anti-mouse IgG antibody (1:5000, in TBS, Sigma-Aldrich #A0545, RRID:AB_257896, and Sigma-Aldrich #A5278) was added and the membranes left in the solution for 2 h at room temperature. After the wash, the labeling was detected with Luminata Forte (Millipore, WBLUF0500) in a ChemiDoc imaging system (Bio-Rad). Band density was measured using Scion Image software. The ratio between synaptophysin and alpha tubulin density was calculated.

2.8. Statistical analysis

All data were analyzed using GraphPad Prism 5 (GraphPad Software, Inc.). Statistical analyses were performed using two-way analysis of variance (ANOVA) followed by Bonferroni post-test for comparison of all pairs of columns. For the comparison of branch numbers between the 3 main experimental groups, a one-way ANOVA was performed, followed by a multiple-comparison Kruskal-Wallis test. The confidence interval was 95%, and all values were expressed as mean ± standard error of the mean (SEM).

3. Results

3.1. Peripheral nerve injury leads to synapse rearrangement in the lumbar spinal cord and motor deficiency

In order to evaluate the impact of peripheral injury on the pre-synaptic density of the LSC, we searched for general pre-synaptic inputs by immunofluorescence for synaptophysin. Control (uninjured) animals showed intense staining, especially around the motoneuron body (Fig. 2A, yellow arrows). Similar staining was observed 1 DAL in both injury models (Fig. 2C, G, K, yellow arrows), although the synaptophysin intensity decreased from 4 DAL in crushed and transected animals (Fig. 2D, H, K, yellow arrows). Quantitative analysis of the integrated density of pixels around the motoneuron cell body revealed a

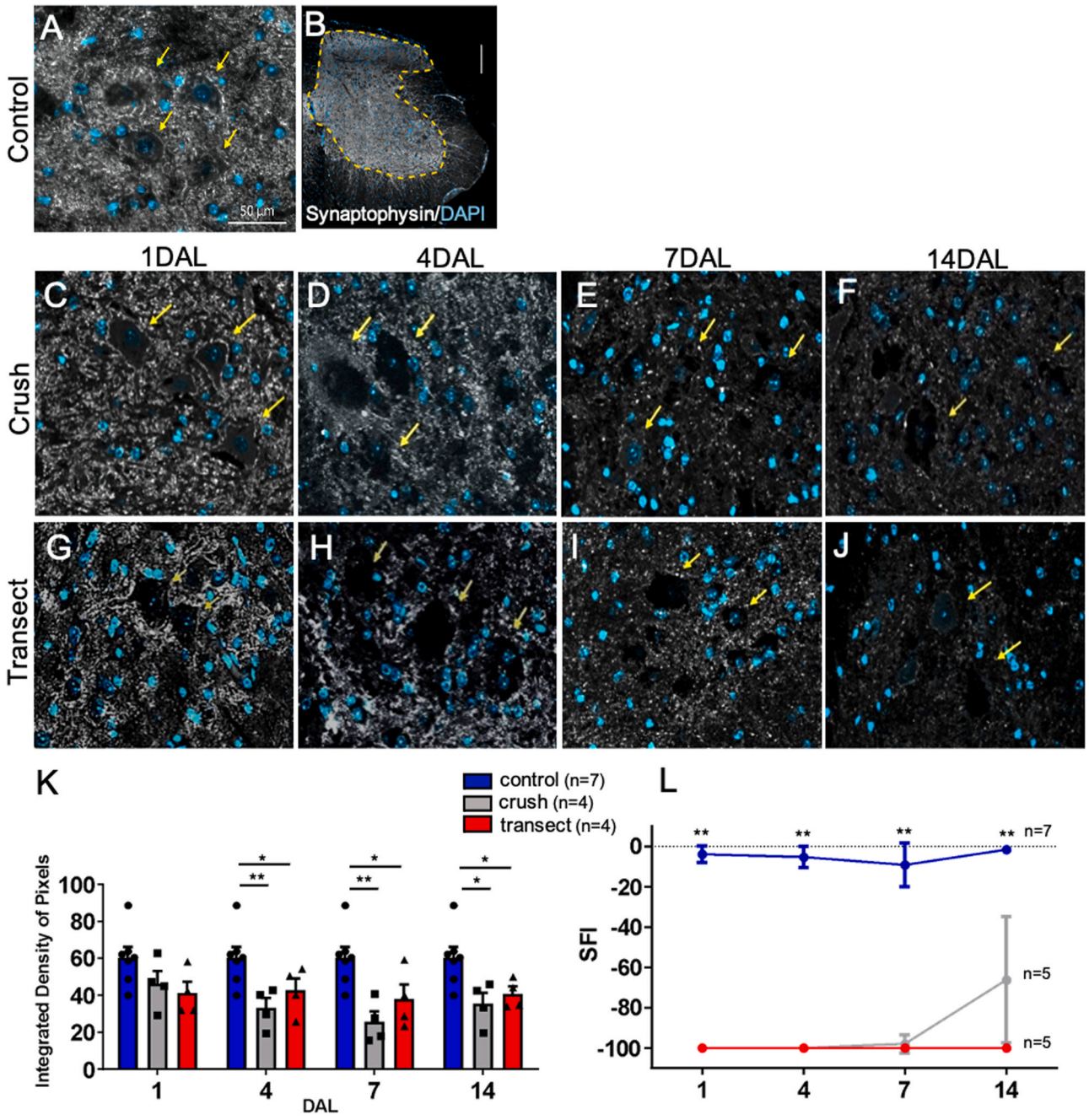

Fig. 2. Synaptophysin-staining decreases around motoneurons after sciatic injury. Images taken from LSC transverse sections (ipsilateral to the nerve injury) in the ventral horn immunolabeled for synaptophysin (white) and nuclei counterstained with DAPI (blue). Animals with crushed nerves (C–F) and transected nerves (G–J) 1, 4, 7, and 14 days after lesion (DAL). Image of ventral horn from uninjured animal (control) at medium (A) and low (B) magnification (contour of spinal cord white matter indicated by dotted yellow line). Soma of motoneurons indicated by yellow arrows. Quantitative analysis of integrated density of pixels surrounding motoneurons in all experimental conditions and DAL (K). Graph of sciatic function index (SFI) analysis obtained by walking-track test (L). Statistics: Two-way ANOVA, Tukey's post-test. $^{*}p < 0.05$ and $^{**}p < 0.005$. For synaptophysin analysis, Control $n = 7$, Crush n = 4/DAL (total 16), Transection $n = 4$/DAL (total 16). For walking track, Control $n = 4$, Crush $n = 5$/DAL (total 20), Transection $n = 5$/DAL (total 20). Scale bars: A, C–$J = 50$ µm; $B = 100$ µm.

significant decrease of synaptophysin in both injury models, starting from 4 DAL (Fig. 2K). We also investigated whether the reduction in synaptophysin after nerve transection or crush would be sustained over 7 (Fig. 2E, I) and 14 days after nerve injury. We did not observe significantly modified levels between the lesioned groups at either time point (Fig. 2K). To correlate molecular changes with motor behavior, the mice were challenged in the CatWalk system and the sciatic function index (SFI) was calculated. All injured animals displayed a lower SFI score until 4 DAL (mean injured = –100, mean controls = –5.14), which might be correlated with paw blockade in the plantar position and the impossibility of supporting the body weight. This behavior was observed over the next 2 weeks in transected animals, but not in crush ones, which showed a significant improvement over the same period (Fig. 2L).

3.2. *Microglial cells increase in number in response to both types of peripheral injury*

Microglial cells are involved in synaptic plasticity during development and critical ages. For that reason, we asked whether these cells might be related to a synaptic decrease in the LSC. Iba-1+ cells in the

spinal cord ipsilateral to the nerve lesion were counted to determine the final cell number after sciatic nerve lesion. The expression of Iba-1 and the number of Iba-1-positive cells gradually increased over the time points up to day 7 (Fig. 3A–P). Microglial cells concentrated mainly in the dorsal spinal cord (Fig. 3A–H and Q) and around motoneuron cell bodies (Fig. 3I–Q, yellow arrows). This can be correlated with the functions of neurons from the dorsal and ventromedial horn to receive information and to project axons toward the spinal nerve, respectively.

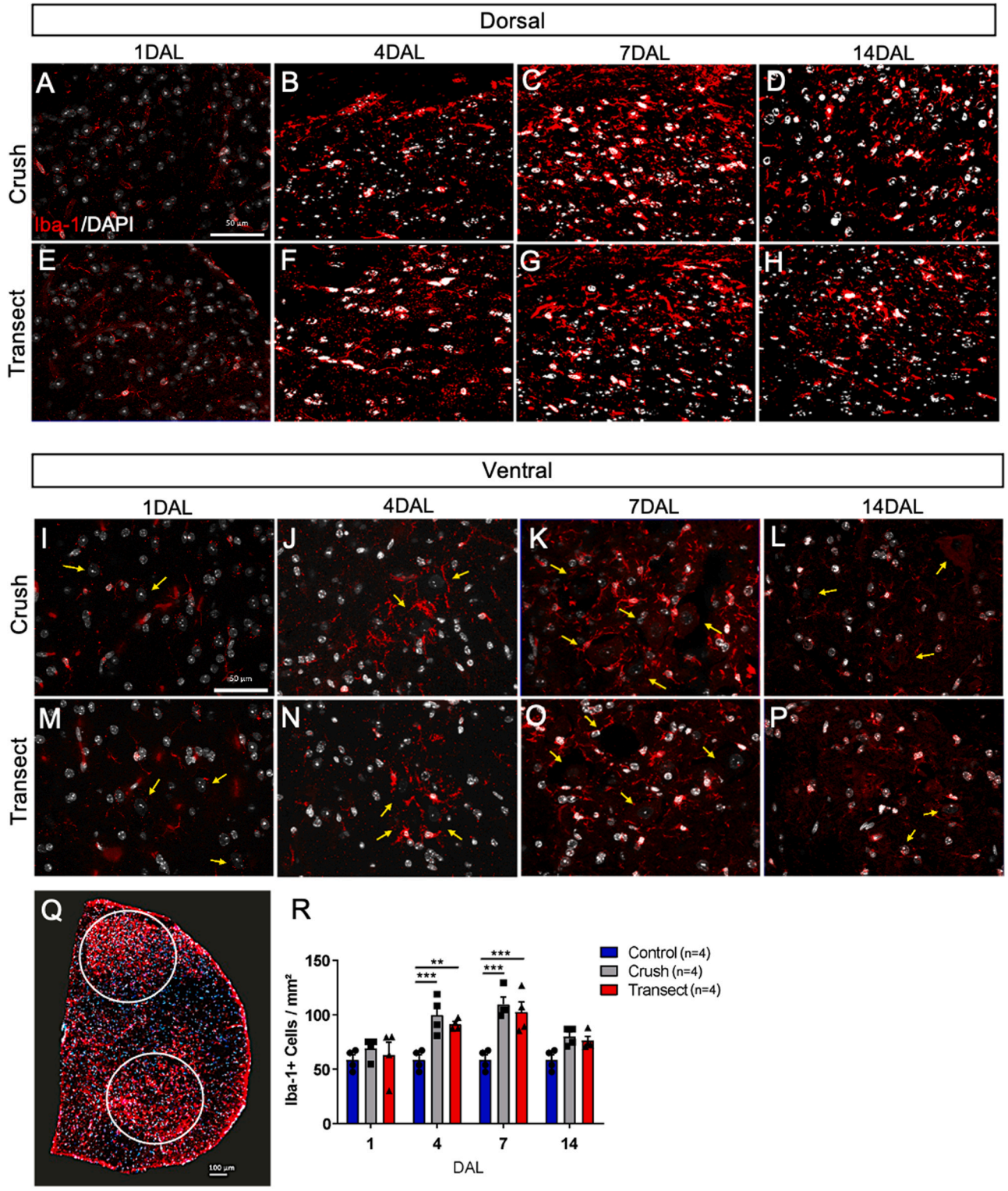

Fig. 3. Microglia recruitment in dorsal and ventral spinal cord horns after nerve injury. Images obtained by apotome microscopy of transverse sections from LSC ipsilateral to nerve injury, immunolabeled for Iba-1 (red) and counterstained with DAPI (white) in dorsal and ventral horns from crush (A–D, I–L) and transected (E–H, M–P) groups 1, 4, 7, and 14 days after lesion (DAL). Low magnification (20×) of LSC ipsilateral to lesion stained for Iba-1 (red) and DAPI (blue) (Q). Histogram of quantitative analysis comparing microglia density in all LSC ipsilateral to nerve injury (Iba-1^{+}) (R). Control $n = 4$, Crush $n = 4$/DAL (total 16), Transection $n = 4$/DAL (total 16). Statistics: Two-way ANOVA, $^{**}p < 0.005$ and $^{***}p < 0.001$. Scale bars: A–P = 50 µm; Q = 100 µm.

One day after lesion (crush or transection animals), there were no significant differences compared to the control (Fig. 3R). Microglial cells increased significantly in the LSC, but especially in the dorsal and ventral horns, 4–7 days after lesion in both crushed and transection mice compared to the control mice (Fig. 3B,C,F,G,J,K,N,O,R). On day 14, the number of Iba-1 + cells decreased, although remaining above the number of control animals (Fig. 3D,H,L,P,R).

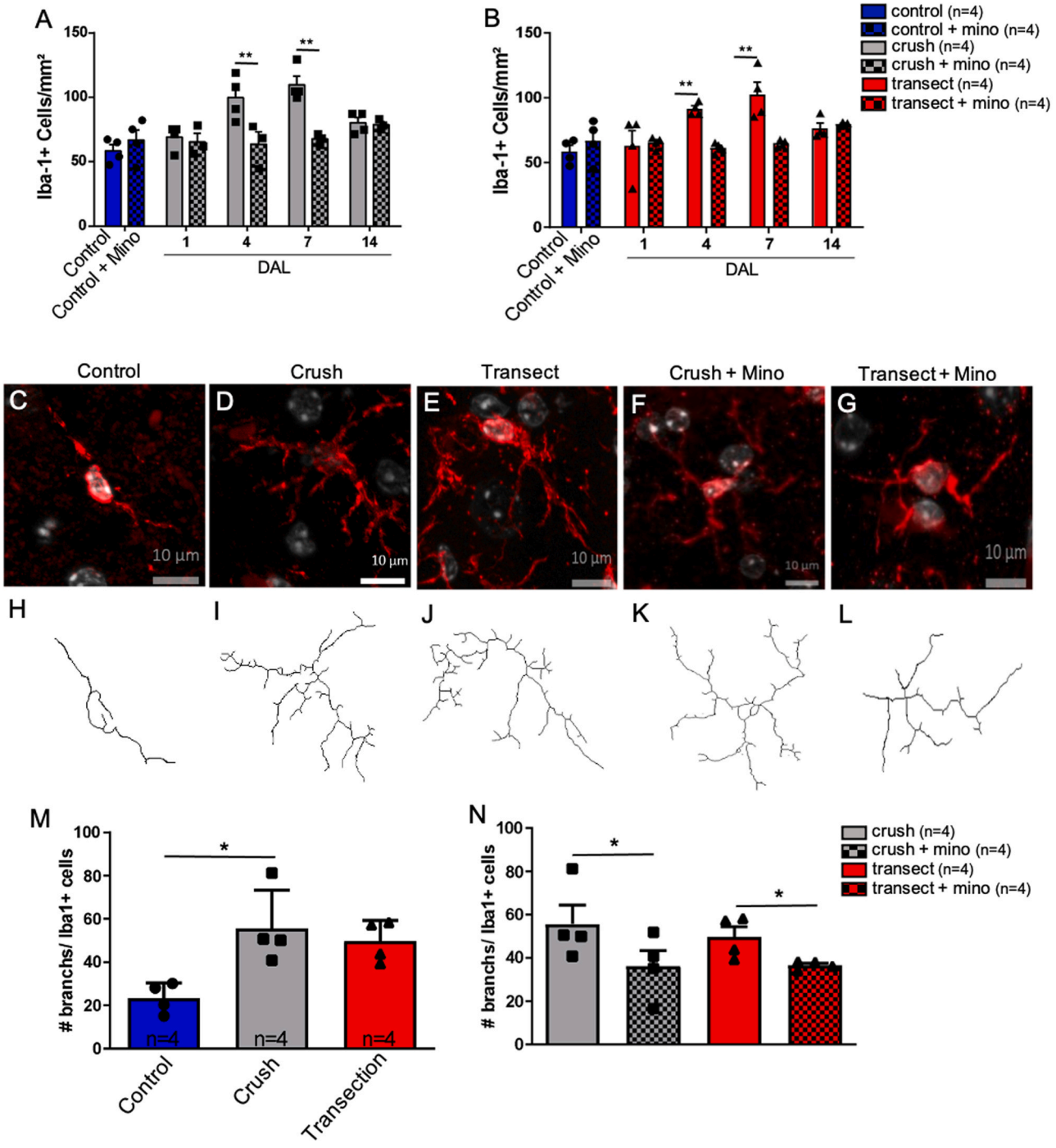

Fig. 4. Microglia recruitment in acute periods after nerve injury is reversed by minocycline in both injury types. Quantitative analysis of Iba-1-positive cells by images taken with apotome microscopy of LSC ipsilateral to nerve injury following minocycline treatment in Crushed (A) and Transected (B) animals. Images taken by apotome at high magnification of LSC transverse sections in ventral horn, of Iba-1-positive microglial cells (red) of uninjured (Control, C), Crush (D), Transection (E), Crush + minocycline (F), and Transection + minocycline (G) animals 7DAL. Nuclei in white were counterstained with DAPI (white). 3D branching reconstruction using ImageJ, from uninjured (Control, H), Crush (I), Transection (J), Crush plus minocycline (K), and Transection plus minocycline (L) animals. Histograms of quantitative analysis comparing the number of microglial branches (M,N). For microglia quantification: Control $n = 4$, Control+Mino $n = 4$; Crush $n = 4$/DAL (total 16), Crush+Mino $n = 4$/DAL (total 16); Transection $n = 4$/DAL (total 16), Transection+Mino $n = 4$/DAL (total 16). For morphological analysis: Control $n = 4$, Control+Mino $n = 4$; Crush $n = 4$, Crush+Mino $n = 4$; Transection $n = 4$, Transection+Mino $n = 4$. Statistics: Two-way ANOVA, $^{*}p < 0.05$ and $^{**}p < 0.005$ for graphs A and B; One-way ANOVA, $^{*}p < 0.05$ for graphs M and N. Scale bars: C–G = 10 µm.

3.3. Microglial cell density and morphology are attenuated by minocycline treatment in acute periods

As described above, the injured animals showed a significant increase in microglial cell number 4 and 7 days after a crush or transection lesion (Fig. 3R). We also investigated whether minocycline treatment could change the microglial density profile in the LSC after nerve lesion. In injured mice (both crushed and transected) treated with minocycline, the microglial cell number did not increase at 4 and 7 DAL, compared to injured animals not treated with the drug (Fig. 4 A and B; Supplementary Figure 1 A–P). Also, the use of minocycline only did not lead to changes in microglial density, since there was no statistical difference between the Control and Control+Mino groups (Fig. 4A and B; Supplementary Figure 1 Q and R). Microglial cells are able to sense a disturbance in the microenvironment, due to the reduced connectivity of the neurons to the peripheral targets after an axonal cut. This is often shown by changes in their morphology. Since the most significant change in microglial cell number was found 7 days after lesion, we analyzed the changes in the microglial phenotype in the LSC ventral horn at this time point. Injured animals showed a highly ramified morphology, in contrast to the microglial cells of uninjured animals (Fig. 4C–E; H–J and M). Since microglial density increases significantly after nerve lesion, we asked whether these observations could be correlated with a reduction in synaptophysin staining. However, first we asked whether daily treatment of mice with minocycline could reverse the ramified morphology induced by nerve lesion. On day 7, we found significant morphological differences between microglial cells in Crush+Mino and Transection+Mino, especially in the number of branches (Fig. 4D–G; I–L). Quantitative analysis confirmed that Crush+Mino and Transection+Mino animals had significantly fewer branches compared to the respective untreated groups (Fig. 4N). Microglial morphological changes after injury and minocycline administration were confirmed by Sholl analysis (Supplementary Fig. 2), where both crushed and transected animals showed significantly more ramified microglia in LSC, especially 10–12.5 μm from the cell body. Also, minocycline significantly reduced ramification in a range of 10 μm starting at 7.5 μm from the cell body. Taken together, these morphological observations demonstrated that both nerve-injury models can modify microglial reactivity in the LSC, and that this reactivity can be attenuated by minocycline treatment.

3.4. Changes in microglial response are correlated with changes in synaptic density

The correlation between microglia cell activity and synapse pruning is well understood; however, the effects of different types of nerve injury on this process remain unclear. Based on the experimental models described above, in this set we analyzed a transverse section of the LSC, aiming to correlate the microglial response and synaptic density after nerve crush or transection under minocycline administration. Over a two-week period after lesion, we observed a significant decrease in synaptophysin immunostaining surrounding the motoneurons in both types of nerve lesion. Quantitative analysis of fluorescent dots confirmed these observations (Fig. 5A and B). Curiously, minocycline treatment did not modify the synaptic density surrounding motoneurons at all time points investigated. Also, administration of minocycline itself did not change the expression of synaptophysin, since there was no statistically significant difference between the Control and Control+Mino animals (Fig. 5A and B).

To analyze the synaptic density in the whole LSC tissue, we investigated the synaptophysin levels in L4–L6 tissue samples by western blotting (Fig. 5C, D). Under the same experimental conditions, the quantitative analysis demonstrated that on day 4 in both injury types, as well as on day 7 in transected nerves, minocycline was correlated with high levels of synaptophysin. These high levels were absent in the untreated group (Fig. 5E, F). There was no significant difference between control mice treated or not with minocycline, reinforcing that the difference in levels of synaptophysin between the injured groups was not directly caused by this drug.

Despite the differences observed in pre-synapse element staining, we found no correlation with motor performance in the CatWalk apparatus. Minocycline-treated mice did not perform better (as assessed by the SFI) than the untreated group, despite a slight visual difference. The marked motor deficits in the transected mice compared to the crushed mice were maintained on day 14, even after treatment with minocycline (Fig. 5G). Taken together, these observations suggest that the synaptic pruning associated with microglia activity is not locally modified with minocycline treatment. Instead, systemic microglia blockage seems to raise regional synapse levels (L4–L6), but not locally as could be expected.

4. Discussion

Peripheral nerve injuries lead to homeostatic disturbances in the central nervous system (CNS) (Wolpaw and Carp, 2006; Navarro et al., 2007). Muscle and skin deafferentation induce a modified somatotopic representation in the cerebral cortex as well as in the spinal cord (Jones, 2000). Similar patterns are observed when axons regenerate and locate their original targets after a PNS injury, leading to a second wave of synaptic plasticity in the CNS (Wall et al., 1984). The different expression of adhesion molecules and neuroligins in the spinal cord after crush or transection nerve lesion has also been described (Thornton et al., 2008; Zelano et al., 2009), although the description of the glial or microglial reaction has not been evaluated. We therefore asked whether different PNS lesions would cause different degrees of synaptic plasticity in the LSC. We compared two types of sciatic injury, crush and transection. Crush injury has been described previously, as a model in which axons can regrow by 7 days after injury (Ribeiro-Resende et al., 2007, 2014). The transection model, involving removal of a 4-mm section of nerve, prevents regeneration through the distal stump and also prevents reinnervation (Aldskogius and Kozlova, 1998; Emirandetti et al., 2006). We confirmed this description, observing that crushed mice partially regained their motor abilities, as assessed by walking-track analysis, by the first and second weeks after sciatic injury, whereas the transected mice did not. These observations supported the validity of our experimental models and allowed us to investigate possible homeostatic changes in the LSC.

Synaptic changes in the spinal cord after PNS nerve lesion involved shrinkage of synaptic inputs, especially around motoneurons, as frequently observed. The reason for these observations might be correlated with a loss of function and degeneration of disrupted axons (Navarro et al., 2007; Svensson and Aldskogius, 1993). We also observed a marked decrease in the synaptic inputs around motoneuron cell bodies in both types of lesions. The beginning of this process seemed to be conserved in both crush and transection on day 4 after lesion; this agrees with previous data showing reduced levels of synaptophysin, synapsin, VGLUT1, and GAD65 a few days after sciatic injury (Emirandetti et al., 2010; Spejo et al., 2013; Arbat-Plana et al., 2015). The hypothesis that different pre-synapse reorganizations occur after different types of nerve lesion was not confirmed. This was supported by our observation of synaptophysin levels and distribution (Fig. 2). Indeed, in the acute period after injury, the nerve regeneration represented by Wallerian degeneration was similar. This might be explained by a massive axonal disruption, not only from the transection itself but also after a strong and maintained compressive nerve lesion (Seddon, 1943; Sunderland, 1951).

It is well established that synaptic rearrangement in the spinal cord is accompanied by reactive gliosis. In this scenario, microglial cells drive their phenotype toward proinflammatory cells (Aldskogius and Kozlova, 1998; Aldskogius, 2011; Tyzack et al., 2014; Terayama et al., 2016).

In both models of sciatic injury, the number of microglial cells increased in the LSC ipsilateral from the nerve injury from 4 to 7 DAL, which can be correlated with a reduction of pre-synaptic elements.

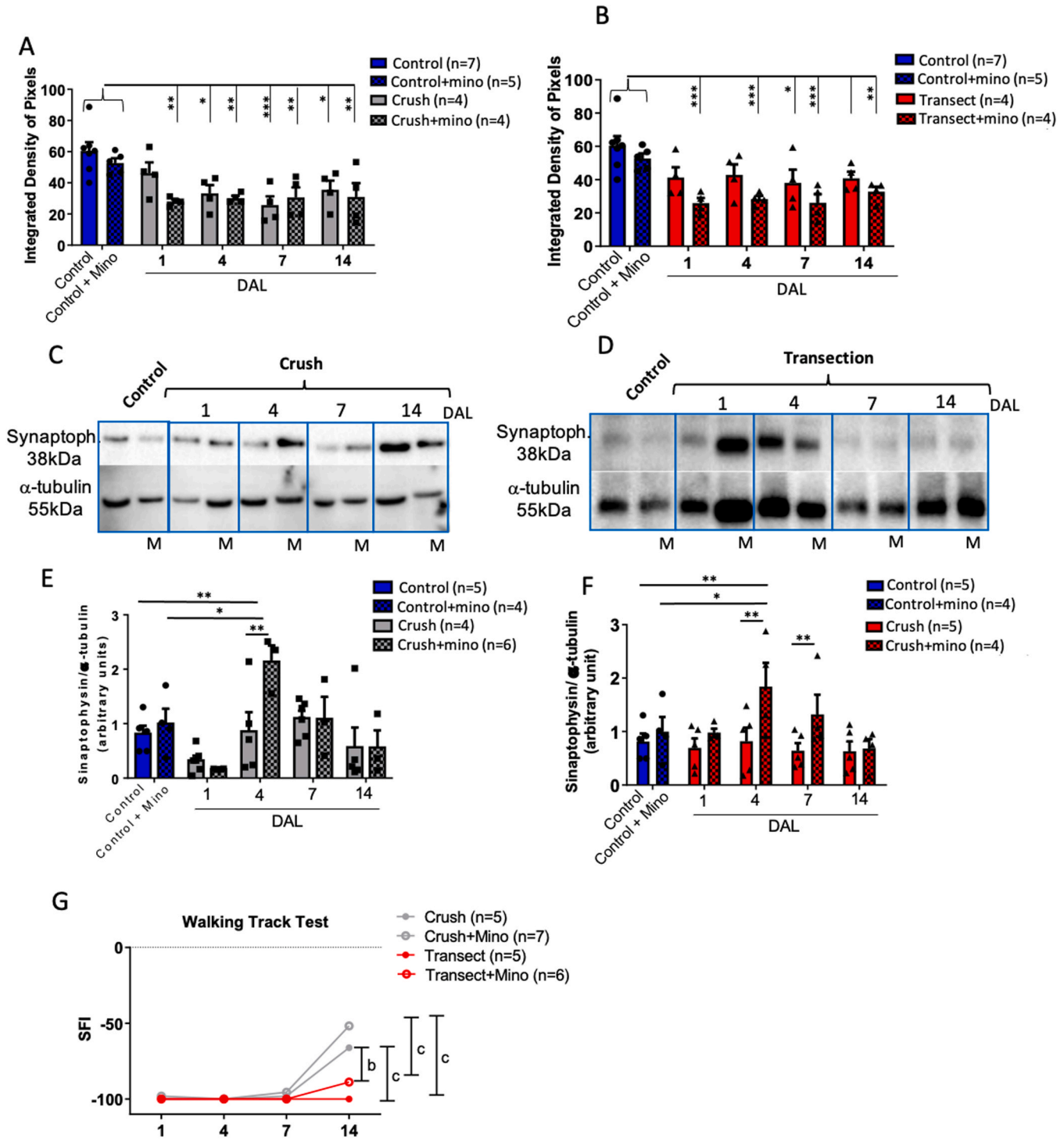

Fig. 5. Minocycline treatment alters synaptophysin expression in LSC after crush and transection sciatic-nerve lesion. Histograms of quantitative analysis of synaptophysin in an integrated density of pixels surrounding motoneurons from groups treated or not with minocycline (A–B). Immunoblots for synaptophysin (38kD) and alpha tubulin (42kD) from LSC tissue dissected from L4–L6 region. Membrane with LSC samples of unlesioned, after nerve crush, and nerve crush + minocycline groups (C) 1, 4, 7, and 14 days after lesion. Membrane with LSC samples of unlesioned, after nerve transection, and nerve transection + minocycline groups (D) 1, 4, 7, and 14 days after lesion. M indicates minocycline treatment in C and D. Histograms of quantitative analysis of synaptophysin:alpha-tubulin density ratio measured by immunoblots, represented in arbitrary units for crushed nerves (E), transected nerves (F), and treated or not with minocycline. Graph of sciatic-function index (SFI) scores of injured animals treated or not with minocycline (G). For synaptophysin immunofluorescence analysis, Control $n = 7$, Control+Mino $n = 5$; Crush $n = 4$/DAL (total 16), Crush+Mino $n = 4$/DAL (total 16); Transection $n = 4$/DAL (total 16), Transection+Mino $n = 4$/DAL (total 16). For synaptophysin western-blotting analysis, Control $n = 5$, Control+Mino $n = 4$; Crush $n = 4$/DAL (total 16), Crush+Mino $n = 6$/DAL (total 24); Transection $n = 5$/DAL (total 20), Transection+Mino $n = 4$/DAL (total 16). For walking track, Crush $n = 5$/DAL (total 20), Crush+Mino $n = 7$/DAL (total 21); Transection $n = 5$/DAL (total 20), Transection+Mino $n = 6$/DAL (total 24). Statistics: Two-way ANOVA, $*p < 0.05$, $**p < 0.005$, $***p < 0.001$.

Additionally, the location of microglial cells around motoneuron cell bodies matched the region where we observed the decrease of synaptic inputs. The physical interaction between the microglia and motoneuron soma provides evidence that the microglia might be involved in regulating synaptophysin levels, therefore moderating the synaptic density. This hypothesis is supported by recent data from Rotterman and Alvarez (2020), who described a significant increase in lysosomes in microglial cells located around motoneurons, 3–14 days after sciatic transection.

Although both types of nerve injury led to a microglial reaction in the spinal cord, similarly to their behavior after a direct CNS injury, we did not observe the characteristic ameboid morphology (data not shown). Calcia and colleagues (2016) reported that microglia exhibit a hypertrophic soma and branches in a chronic inflammatory process. This also correlates with the present consensus regarding the range of microglial phenotype and morphology, so that these cells ramify in homeostasis or become ameboid during an insult (Colton, 2009; Walker et al., 2014).

We quantified the number of microglial branches. In the acute period after a sciatic crush or transection, the number of branches increased significantly compared to the number in the homeostatic spinal cord (control group). This profile agrees with the morphological changes described by Yamada and Jinno (2013), where microglial cells in the hypoglossal nucleus migrated and ramified after hypoglossal nerve axotomy. Another study that evaluated microglial morphology in the spinal cord after sciatic injury described the increase of hyperpolarized and ramified microglia 7 days after lesion, with no description of ameboid cells, i.e., no branching (Zhang et al., 2008).

Based on the clear reactivity of microglial cells after sciatic-nerve injury, we modulated the microglial reactivity pharmacologically, based on previous successful protocols for spinal cord investigations (Yrjänheikki et al., 1998; Nikodemova et al., 2007; Li et al., 2016). Daily treatment with minocycline prevented the number of microglial cells in the spinal cord from increasing after injury, although we still observed Iba-1-positive cells around motoneurons (Supplementary Figure 1). The continuous presence of microglia in this spinal cord area may explain why we did not observe a difference in synaptophysin staining around motoneurons between injured mice treated or not with minocycline. Nevertheless, the effect of minocycline on the microglial response to injury agreed with previous observations and did not affect either the microglia population or the synapse protein levels in uninjured mice (Nikodemova et al., 2007; Popiolek-Barczyk et al., 2014; Li et al., 2016).

Peripheral nerve injury leads to astrocyte reactivity, and this reactivity participates in synapse rearrangement (Emirandetti et al., 2006; Tyzack et al., 2014). Also, it has been reported that not only do astrocytes react in a different time window than microglia, but also that they are not directly influenced by minocycline (Yrjänheikki et al., 1998; Rojewska et al., 2014; Liang et al., 2016; Terayama et al., 2016). Therefore, the decrease in synaptophysin labeling in the ventral horn area might be a consequence of the astrocyte response.

In contrast, the quantification of synaptophysin through western blotting revealed significantly increased levels of this protein 4 and 7 DAL in the injured groups treated with minocycline. Importantly, the histological analysis around motoneurons evaluated only a small portion of the spinal cord, while for the western-blot procedure we used the whole spinal cord from L4–L6. So, this molecular approach includes other active plastic areas from the LSC, such as the dorsal horn, which is also an area where we observed microglial reactivity (Fig. 3). The increase in the size of the samples may be one of the reasons why the difference in synaptophysin level between the experimental groups was more evident. Also, as Woolf et al. (1995) and Sun et al. (2006) described, while there is a decrease of pre-synaptic elements in the ventral horn, new synapses are formed in the dorsal horn, increasing the expression of synaptic proteins and synaptophysin in that area. Finally, minocycline has been evaluated not only for its capacity to reduce Iba-1, but also components of the complement system such as C1q (Rojewska et al., 2014), which are associated with synaptic pruning. Indeed, other groups have demonstrated that the complement system is involved in the mechanisms related to synaptic pruning in the spinal cord after nerve injury (Berg et al., 2012). This involvement may be another mechanism by which minocycline could modulate synaptic pruning.

Taken together, our observations confirmed that minocycline is a useful tool for modulating the microglial response, although the treatment was not able to completely suppress the cell response. Our findings for the changes in presynaptic element staining in the LSC after a peripheral nerve lesion, and the subsequent modulation of the microglia reaction, will lead to further investigations of nerve regeneration by optimizing spinal cord stability during the nerve degenerative process. Another question to address in the near future is whether similar effects of both types of nerve injury on acute spinal plasticity in male mice could be reproducible in female mice. The importance of this issue is supported by the observations that microglial cells can behave differently in each sex and that this different behavior affects the synaptic (Weinhard et al., 2018; Szabo-Pardi et al., 2021).

5. Conclusion

Here, we demonstrated that both crush and transection of the sciatic nerve led to the recruitment of microglial cells in regions near motoneurons in the LSC, and that this was correlated with pruning of synaptic elements. Systemic minocycline treatment reduced the number of microglia and affected their morphology. These observations were correlated with a partial blockage of synaptic pruning at the L4–L6 spinal cord level.

CRediT authorship contribution statement

Raquel M.P. Campos: Conceptualization, Methodology, Data curation, Project administration, Formal analysis, Investigation, Writing - original draft, Writing - review & editing. **Maria Carolina Barbosa-Silva**: Methodology, Data curation, Formal analysis, Investigation. **Victor T. Resende**: Conceptualization, Methodology, Data curation, Project administration, Writing - original draft, Writing - review & editing, Funding acquisition.

Acknowledgements

The authors are grateful to Luciano Cavalcante for laboratory technical support.

Authors' contributions

RMPC: Performed all the animal handling experiments, tissue processing, immunolabeling and quantitative analysis, analyzed data, imaging by optical microscopy, wrote and discuss the manuscript. MCBS: Performed tissue processing, tissue immunolabeling and analyzed data. VTRR: General coordinator, analyzed data, wrote the manuscript, performed statistical analysis and imaging by optical microscopy.

Funding acknowledgements

This study was supported by the Coordenação de Aperfeiçoamento de Pessoal de Nível Superior (CAPES), Fundação Carlos Chagas Filho de Amparo à Pesquisa do Estado do Rio de Janeiro (FAPERJ), and Conselho Nacional de Desenvolvimento Científico e Tecnológico (CNPq), all to VTRR.

Authors' declaration

Declarations of interest: none.

Appendix A. Supporting information

Supplementary data associated with this article can be found in the

online version at doi:10.1016/j.ibneur.2021.05.002.

References

Ahmed, A., Wang, L.L., Abdelmaksoud, S., Aboelgheit, A., Saeed, S., Zhang, C.L., 2017. Minocycline modulates microglia polarization in ischemia-reperfusion model of retinal degeneration and induces neuroprotection. Sci. Rep. 7 (1), 14065.

Aldskogius, H., 2011. Mechanisms and consequences of microglial responses to peripheral axotomy. Front. Biosci. 3, 857–868.

Aldskogius, H., Kozlova, E.N., 1998. Central neuron-glial and glial-glial interactions following axon injury. Prog. Neurobiol. 55 (1), 1–26.

Alvarez, F.J., Titus-Mitchell, H.E., Bullinger, K.L., Kraszpulski, M., Nardelli, P., Cope, T. C., 2011. Permanent central synaptic disconnection of proprioceptors after nerve injury and regeneration. I. Loss of VGLUT1/IA synapses on motoneurons. J. Neurophysiol. 106 (5), 2450–2470.

Arbat-Plana, A., Torres-Espín, A., Navarro, X., Udina, E., 2015. Activity dependent therapies modulate the spinal changes that motoneurons suffer after a peripheral nerve injury. Exp. Neurol. 263, 293–305.

Bastien, D., Lacroix, S., 2014. Cytokine pathways regulating glial and leukocyte function after spinal cord and peripheral nerve injury. Exp. Neurol. 258, 62–77.

Berg, A., Zelano, J., Stephan, A., Thams, S., Barres, B.A., Pekny, M., Pekna, M., Cullheim, S., 2012. Reduced removal of synaptic terminals from axotomized spinal motoneurons in the absence of complement C3. Exp. Neurol. 237 (1), 8–17.

Biber, K., Neumann, H., Inoue, K., Boddeke, H.W., 2007. Neuronal 'On' and 'Off' signals control microglia. Trends Neurosci. 30 (11), 596–602.

Blinzinger, K., Kreutzberg, G., 1968. Displacement of synaptic terminals from regenerating motoneurons by microglial cells. Zeitschrift fur Zellforschung und mikroskopische Anatomie 85 (2), 145–157.

Calcia, M.A., Bonsall, D.R., Bloomfield, P.S., Selvaraj, S., Barichello, T., Howes, O.D., 2016. Stress and neuroinflammation: a systematic review of the effects of stress on microglia and the implications for mental illness. Psychopharmacology 233 (9), 1637–1650.

Colton, C.A., 2009. Heterogeneity of microglial activation in the innate immune response in the brain. J. Neuroimmune Pharmacol. 4 (4), 399–418.

Emirandetti, A., Zanon, R.G., Sabha Jr., M., de Oliveira, A.L.R., 2006. Astrocyte reactivity influences the number of presynaptic terminals opposed to spinal motoneurons after axotomy. Brain Res. 1095 (1), 35–42.

Emirandetti, A., Simões, G.F., Zanon, R.G., Oliveira, A.L., 2010. Spinal motoneuron synaptic plasticity after axotomy in the absence of inducible nitric oxide synthase. J. Neuroinflamm. 7, 31.

Ginhoux, F., Greter, M., Leboeuf, M., Nandi, S., See, P., Gokhan, S., Mehler, M.F., Conway, S.J., Ng, L.G., Stanley, E.R., Samokhvalov, I.M., Merad, M., 2010. Fate mapping analysis reveals that adult microglia derive from primitive macrophages. Science 330 (6005), 841–845. https://doi.org/10.1126/science.1194637.

Gomez-Nicola, D., Perry, V.H., 2015. Microglial dynamics and role in the healthy and diseased brain: a paradigm of functional plasticity. Neuroscientist 21 (2), 169–184.

Hundeshagen, G., Szameit, K., Thieme, H., Finkensieper, M., Angelov, D.N., Guntinas-Lichius, O., Irintchev, A., 2013. Deficient functional recovery after facial nerve crush in rats is associated with restricted rearrangements of synaptic terminals in the facial nucleus. Neuroscience. 248, 307–318.

Inserra, M.M., Bloch, D.A., Terris, D.J., 1998. Functional indices for sciatic, peroneal, and posterior tibial nerve lesions in the mouse. Microsurgery 18 (2), 119–124.

Jones, E.G., 2000. Cortical and subcortical contributions to activity-dependent plasticity in primate somatosensory cortex. Annu. Rev. Neurosci. 23, 1–37.

Jones, R.S., Lynch, M.A., 2015. How dependent is synaptic plasticity on microglial phenotype? Neuropharmacology 96 (A), 3–10.

Li, Z., Wei, H., Piirainen, S., Chen, Z., Kalso, E., Pertovaara, A., Tian, L., 2016. Spinal versus brain microglial and macrophage activation traits determine the differential neuroinflammatory responses and analgesic effect of minocycline in chronic neuropathic pain. Brain Behav. Immun. 58, 107–117.

Liang, Y., Qiu, Y., Du, J., Liu, J., Fang, J., Zhu, J., Fang, J., 2016. Inhibition of spinal microglia and astrocytes contributes to the anti-allodynic effect of electroacupuncture in neuropathic pain induced by spinal nerve ligation. Acupunct. Med. 34 (1), 40–47.

Lisi, L., Ciotti, G.M., Braun, D., Kalinin, S., Currò, D., Dello Russo, C., Coli, A., Mangiola, A., Anile, C., Feinstein, D.L., Navarra, P., 2017. Expression of iNOS, CD163 and ARG-1 taken as M1 and M2 markers of microglial polarization in human glioblastoma and the surrounding normal parenchyma. Neurosci. Lett. 645, 106–112.

Mecha, M., Carrillo-Salinas, F.J., Feliú, A., Mestre, L., Guaza, C., 2016. Microglia activation states and cannabinoid system: therapeutic implications. Pharmacol. Ther. 166, 40–55.

Navarro, X., Vivó, M., Valero-Cabré, A., 2007. Neural plasticity after peripheral nerve injury and regeneration. Prog. Neurobiol. 82 (4), 163–201.

Nikodemova, M., Watters, J.J., Jackson, S.J., Yang, S.K., Duncan, I.D., 2007. Minocycline down-regulates MHC II expression in microglia and macrophages through inhibition of IRF-1 and protein kinase C (PKC)alpha/betaII. J. Biol. Chem. 282 (20), 15208–15216.

Orihuela, R., McPherson, C.A., Harry, G.J., 2016. Microglial M1/M2 polarization and metabolic states. Br. J. Pharmacol. 173 (4), 649–665.

Popiolek-Barczyk, K., Rojewska, E., Jurga, A.M., Makuch, W., Zador, F., Borsodi, A., Piotrowska, A., Przewlocka, B., Mika, J., 2014. Minocycline enhances the effectiveness of nociceptin/orphanin FQ during neuropathic pain. Biomed. Res. Int. 2014, 762930.

Prinz, M., Priller, J., Sisodia, S.S., Ransohoff, R.M., 2011. Heterogeneity of CNS myeloid cells and their roles in neurodegeneration. Nat. Neurosci. 14 (10), 1227–1235.

Ribeiro-Resende, V.T., Oliveira-Silva, A., Ouverney-Brandão, S., Santiago, M.F., Hedin-Pereira, C., Mendez-Otero, R., 2007. Ganglioside 9-O-acetyl GD3 expression is upregulated in the regenerating peripheral nerve. Neuroscience 147 (1), 97–105.

Ribeiro-Resende, V.T., Araújo Gomes, T., de Lima, S., Nascimento-Lima, M., Bargas-Rega, M., Santiago, M.F., Reis, R.A., de Mello, F.G., 2014. Mice lacking GD3 synthase display morphological abnormalities in the sciatic nerve and neuronal disturbances during peripheral nerve regeneration. PLoS One 9 (10), 108919.

Rojewska, E., Popiolek-Barczyk, K., Jurga, A.M., Makuch, W., Przewlocka, B., Mika, J., 2014. Involvement of pro- and antinociceptive factors in minocycline analgesia in rat neuropathic pain model. J. Neuroimmunol. 277 (1–2), 57–66.

Rotterman, T.M., Akhter, E.T., Lane, A.R., MacPherson, K.P., García, V.V., Tansey, M.G., Alvarez, F.J., 2019. Spinal motor circuit synaptic plasticity after peripheral nerve injury depends on microglia activation and a CCR2 mechanism. J. Neurosci. 39 (18), 3412–3433.

Rotterman, T.M., Alvarez, F.J., 2020. Microglia dynamics and interactions with motoneurons axotomized after nerve injuries revealed by two-photon imaging. Sci. Rep. 10 (1), 8648.

Scholz, R., Sobotka, M., Caramoy, A., Stempfl, T., Moehle, C., Langmann, T., 2015. Minocycline counter-regulates pro-inflammatory microglia responses in the retina and protects from degeneration. J. Neuroinflamm. 12, 209. https://doi.org/10.1186/s12974-015-0431-4.

Schultz, A.J., Rotterman, T.M., Dwarakanath, A., Alvarez, F.J., 2017. VGLUT1 synapses and P-boutons on regenerating motoneurons after nerve crush. J. Comp. Neurol. 525 (13), 2876–2889.

Seddon, H.J., 1943. Three types of nerve injury. Brain 66, 237–288.

Spejo, A.B., Carvalho, J.L., Goes, A.M., Oliveira, A.L., 2013. Neuroprotective effects of mesenchymal stem cells on spinal motoneurons following ventral root axotomy: synapse stability and axonal regeneration. Neuroscience 250, 715–732.

Spittau, B., 2017. Aging microglia-phenotypes, functions and implications for age-related neurodegenerative diseases. Front. Aging Neurosci. 9, 194.

Stevens, B., Allen, N.J., Vazquez, L.E., Howell, G.R., Christopherson, K.S., Nour, N., Micheva, K.D., Mehalow, A.K., Huberman, A.D., Stafford, B., Sher, A., Litke, A.M., Lambris, J.D., Smith, S.J., John, S.W., Barres, B.A., 2007. The classical complement cascade mediates CNS synapse elimination. Cell 131 (6), 1164–1178.

Stratoulias, V., Venero, J.L., Tremblay, M.È., Joseph, B., 2019. Microglial subtypes: diversity within the microglial community. EMBO J. 38 (17), 101997.

Sun, T., Xiao, H.S., Zhou, P.B., Lu, Y.J., Bao, L., Zhang, X., 2006. Differential expression of synaptoporin and synaptophysin in primary sensory neurons and up-regulation of synaptoporin after peripheral nerve injury. Neuroscience 141 (3), 1233–1245.

Sunderland, S., 1951. A classification of peripheral nerve injures producing loss of function. Brain 74, 491–516.

Svensson, M., Aldskogius, H., 1993. Synaptic density of axotomized hypoglossal motorneurons following pharmacological blockade of the microglial cell proliferation. Exp. Neurol. 120 (1), 123–131.

Szabo-Pardi, T.A., Syed, U.M., Castillo, Z.W., Burton, M.D., 2021. Use of integrated optical clearing and 2-photon imaging to investigate sex differences in neuroimmune interactions after peripheral nerve injury. Front. Cell Dev. Biol. 9, 624201 https://doi.org/10.3389/fcell.2021.624201.

Terayama, R., Yamamoto, Y., Kishimoto, N., Tabata, M., Maruhama, K., Iida, S., Sugimoto, T., 2016. Differential changes in neuronal excitability in the spinal dorsal horn after spinal nerve ligation in rats. Neurochem. Res. 41 (11), 2880–2889.

Thornton, M.R., Shawcross, S.G., Mantovani, C., Kingham, P.J., Birchall, M.A., Terenghi, G., 2008. Neurotrophins 3 and 4 differentially regulate NCAM, L1 and N-cadherin expression during peripheral nerve regeneration. Biotechnol. Appl. Biochem. 49 (Pt 2), 165–174.

Trapp, B.D., Wujek, J.R., Criste, G.A., et a, Trapp, B.D., Wujek, J.R., Criste, G.A., Jalabi, W., Yin, X., Kidd, G.J., Stohlman, S., Ransohoff, R., 2007. Evidence for synaptic stripping by cortical microglia. Glia 55 (4), 360–368.

Tyzack, G.E., Sitnikov, S., Barson, D., Adams-Carr, K.L., Lau, N.K., Kwok, J.C., Zhao, C., Franklin, R.J., Karadottir, R.T., Fawcett, J.W., Lakatos, A., 2014. Astrocyte response to motor neuron injury promotes structural synaptic plasticity via STAT3-regulated TSP-1 expression. Nat. Commun. 5, 4294.

Wake, H., Moorhouse, A.J., Jinno, S., Kohsaka, S., Nabekura, J., 2009. Resting microglia directly monitor the functional state of synapses in vivo and determine the fate of ischemic terminals. J. Neurosci. 29 (13), 3974–3980.

Walker, F.R., Beynon, S.B., Jones, K.A., Zhao, Z., Kongsui, R., Cairns, M., Nilsson, M., 2014. Dynamic structural remodelling of microglia in health and disease: a review of the models, the signals and the mechanisms. Brain Behav. Immun. 37, 1–14.

Wall, J.T., Kaas, J.H., Sur, M., Nelson, R.J., Felleman, D.J., Merzenich, M.M., 1986. Functional reorganization in somatosensory cortical areas 3b and 1 of adult monkeys after median nerve repair: possible relationships to sensory recovery in humans. J. Neurosci. 6 (1), 218–233.

Wang, N., Mi, X., Gao, B., Gu, J., Wang, W., Zhang, Y., Wang, X., 2015. Minocycline inhibits brain inflammation and attenuates spontaneous recurrent seizures following pilocarpine-induced status epilepticus. Neuroscience 287, 144–156.

Weinhard, L., Neniskyte, U., Vadisiute, A., di Bartolomei, G., Aygün, N., Riviere, L., Zonfrillo, F., Dymecki, S., Gross, C., 2018. Sexual dimorphism of microglia and synapses during mouse postnatal development. Dev. Neurobiol. 78 (6), 618–626.

Wolpaw, J.R., Carp, J.S., 2006. Plasticity from muscle to brain. Prog. Neurobiol. 78 (3–5), 233–263.

Woolf, C.J., Shortland, P., Reynolds, M., Ridings, J., Doubell, T., Coggeshall, R.E., 1995. Reorganization of central terminals of myelinated primary afferents in the rat dorsal horn following peripheral axotomy. J. Comp. Neurol. 360 (1), 121–134.

Xavier, A.L., Menezes, J.R., Goldman, S.A., Nedergaard, M., 2014. Fine-tuning the central nervous system: microglial modelling of cells and synapses. Philos. Trans. R. Soc. Lond. B Biol. Sci. 369 (1654), 20130593.

Xu, N., Tang, X.H., Pan, W., Xie, Z.M., Zhang, G.F., Ji, M.H., Yang, J.J., Zhou, M.T., Zhou, Z.Q., 2017. Spared nerve injury increases the expression of microglia M1 markers in the prefrontal cortex of rats and provokes depression-like behaviors. Front. Neurosci. 11, 209.

Yamada, J., Jinno, S., 2013. Novel objective classification of reactive microglia following hypoglossal axotomy using hierarchical cluster analysis. J. Comp. Neurol. 521 (5), 1184–1201.

Young, K., Morrison, H., 2018. Quantifying microglia morphology from photomicrographs of immunohistochemistry prepared tissue using ImageJ. J. Vis. Exp. (136), 57648.

Yrjänheikki, J., Keinänen, R., Pellikka, M., Hökfelt, T., Koistinaho, J., 1998. Tetracyclines inhibit microglial activation and are neuroprotective in global brain ischemia. Proc. Natl. Acad. Sci. USA 95 (26), 15769–15774.

Zhang, F., Vadakkan, K.I., Kim, S.S., Wu, L.J., Shang, Y., Zhuo, M., 2008. Selective activation of microglia in spinal cord but not higher cortical regions following nerve injury in adult mouse. Mol. Pain 4, 15. https://doi.org/10.1186/1744-8069-4-15.

Zelano, J., Berg, A., Thams, S., Hailer, N.P., Cullheim, S., 2009. SynCAM1 expression correlates with restoration of central synapses on spinal motoneurons after two different models of peripheral nerve injury. J. Comp. Neurol. 517 (5), 670–682.